



Two-point measurement of entropy production from the outcomes of a single experiment with correlated photon pairs

Gabriel H. Aguilar,¹ Thaís L. Silva ¹, Thiago E. Guimarães,¹ Rodrigo S. Piera,¹ Lucas C. Céleri ² and Gabriel T. Landi^{3,*}

¹Federal University of Rio de Janeiro, Rio de Janeiro, Rio de Janeiro 21941-901, Brazil

²Institute of Physics, Federal University of Goiás, P.O. Box 131, Goiânia, Goiás 74001-970, Brazil

³Instituto de Física, Universidade de São Paulo, São Paulo, São Paulo 05314-970, Brazil



(Received 11 August 2021; revised 20 January 2022; accepted 28 June 2022; published 17 August 2022)

Fluctuation theorems are one of the pillars of nonequilibrium thermodynamics. Broadly speaking, they concern the statistical distribution of quantities such as heat, work, or entropy production. Quantum experiments, however, usually can only assess these distributions indirectly, or reconstruct them *a posteriori*. In this Letter we report an experiment where the distribution of entropy production is obtained directly from the outcomes (clicks) of an optical experiment simulating the interaction between a two-level system and a thermal reservoir. The setup consists of entangled photon pairs, one of which is sent to an interferometer implementing a finite-temperature amplitude damping channel, and is designed so as to allow full access to the two-point measurement statistics of both system and reservoir. First, by measuring the entangled pair, we directly implement the two-point measurement scheme in the system, avoiding the destructive nature of photodetection. Second, each optical path of the interferometer is associated with a specific transition of the reservoir. Thus, by blocking all but one of the paths, we can measure the conditional entropy production, given a specific reservoir trajectory.

DOI: [10.1103/PhysRevA.106.L020201](https://doi.org/10.1103/PhysRevA.106.L020201)

I. INTRODUCTION

In the micro- and mesoscopic domains, thermodynamic quantities such as heat, work, and entropy production may fluctuate significantly. They must therefore be described by random variables, with an associated probability distribution. This change in paradigm has led to ground-breaking new insights in nonequilibrium thermodynamics. One reason in particular was the discovery of fluctuation theorems (FTs), special symmetries of these distributions which generalize the second law of thermodynamics [1–5]. Thermodynamics, however, deals with processes, not states. That is, quantities such as heat or work depend on the *transformations* a system undergoes. Assessing these in an experiment therefore requires measuring the system in (at least) two instants of time. For classical processes, this is generally not an issue [6–8]; however, in the quantum domain, measurements become invasive.

The default protocol for estimating quantum thermodynamic quantities is the two-point measurement (TPM) scheme [9–11] [Fig. 1(a)]. It consists in measuring the system in the energy eigenbasis, before and after the process. This yields a stochastic trajectory of outcomes, $\gamma \rightarrow \gamma'$, from which the corresponding thermodynamic quantities can be computed. Notwithstanding its limitations [13–21], the TPM remains the main methodology for obtaining thermodynamic properties of quantum systems. However, experimentally implementing the two measurements *in sequence* can be extremely challenging: Quantum observables are often only inferred indirectly or via a destructive process, such as photodetection.

Instead, the distribution of outcomes $P(\gamma, \gamma')$ is usually written as $P(\gamma, \gamma') = P(\gamma'|\gamma)P(\gamma)$ and the two terms are determined from separate experiments. This was the case, for instance, in Ref. [22], which was the first to report on quantum fluctuation theorems. In one experiment the system is prepared in some initial state (usually thermal) and the initial probabilities $P(\gamma)$ are measured. Then, in a second experiment one *prepares* a given state γ , runs the process, and then measures it in γ' , thus obtaining the transition probability $P(\gamma'|\gamma)$. The TPM is then reconstructed from postprocessing, with the purpose of confirming the validity of FTs. Similar issues are also found in other platforms, where $P(\gamma)$ is extracted directly from the preparation of the initial thermal state instead of being measured in the first measurement of the TPM [23–25].

In recent years there has been significant progress in developing alternative implementations of the TPM. One approach, used, e.g., in nuclear magnetic resonance experiments [26,27], is based on Ramsey interferometry to indirectly estimate the characteristic function (from which the distribution can be reconstructed via a Fourier transform) [28,29]. Another method is based on the interpretation of work as the direct outcomes of a generalized quantum measurement (positive-operator-valued measure), as put forth in [30]. This was implemented in Ref. [31], to directly measure the work distribution in a quantum gas, without having to resort first to the TPM. Continuous weak measurements have also been used in superconducting circuits [32], as an alternative to the two-point nature of the TPM. The only experiment directly performing the two measurements of the TPM in a single shot is that in Ref. [33], which used nondemolition measurements on superconducting qubits. That setup, however, is restricted to measurements in the system only, being unable to access environmental degrees

*gtlandi@gmail.com

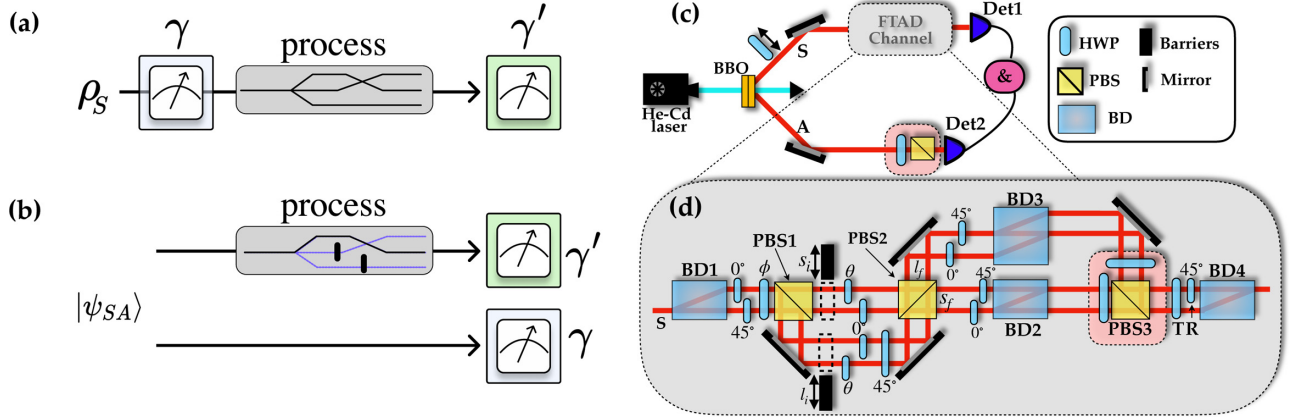


FIG. 1. (a) Standard TPM scheme, which consists in measuring a quantum system before and after a thermodynamic process. The first measurement, with outcome γ , may invasively affect the process and in general is difficult to implement experimentally in a single experimental run. (b) We bypass these issues using two features. First, we distinguish the different configurations of the bath (black and purple lines inside the gray rectangle) by blocking specific arms of the interferometer. Second, we use entangled photon pairs, where only one is sent through the thermodynamic process. Due to the coincidences postselection, measuring the other photon yields information about the initial state, before the process. (c) Experimental setup. Pairs of entangled photons are created using SPDC. The photon in mode S is sent to a FTAD channel, while the photon in mode A is detected after a projective measurement in its polarization. Coincidence counts are registered with detections in Det1 and Det2. (d) Interferometric implementation of the FTAD channel (see the text and Supplemental Material [12] for more details).

of freedom, which are crucial when heat exchange is also involved [34].

In this Letter we report an experiment where both outcomes of a TPM, in both the system and bath, are directly associated with the clicks of a single experiment. We study the entropy production in a system comprising an entangled photon pair, where one of the photons is sent to an interferometer implementing a finite-temperature amplitude damping (FTAD) channel, representing the interaction with a heat bath [35–38]. To perform the TPM, we introduce two features, which are unique to our setup [Fig. 1(b)]. First, each path of the interferometer is mapped into a different bath configuration. Hence, by blocking all but one of the paths, we can measure the statistics conditioned on a given stochastic trajectory of the environment. These are usually very challenging in other platforms, since they require projective measurements on the reservoir, before and after the interaction. Second, we use coincidence counts for measuring both photons in the entangled pair. Detecting the polarization of the photon that went through the interferometer yields γ' . In addition, the outcomes of the entangled pair determine the configuration γ , before the process occurred. This does not have the artificiality of having to measure $P(\gamma)$ in a separate experiment. A similar method, but focused on work protocols, has been reported in [39,40].

II. EXPERIMENTAL SETUP

The experimental setup is shown in Fig. 1(c). A He-Cd laser pumps two β barium borate (BBO) crystals in a crossed axis configuration. By type-I spontaneous parametric down-conversion (SPDC), photon pairs in the entangled state $|\psi_{SA}\rangle = \sqrt{\delta}|00\rangle_{SA} + \sqrt{1-\delta}|11\rangle_{SA}$ are produced in the modes S and A [41], where the computational bases $|0\rangle_{S(A)}$ and $|1\rangle_{S(A)}$ corresponds to the horizontal and vertical polarizations, respectively. The reduced state of S thus reads

$\rho_S = \delta|0\rangle_S\langle 0| + (1-\delta)|1\rangle_S\langle 1|$, which is a thermal state, with occupation δ .

The A photons are detected in an avalanche photon diode (Det2), after polarization projective measurements, implemented by a half waveplate (HWP) and a polarized beam splitter (PBS). Due to the correlated nature of $|\psi_{SA}\rangle$ and the postselection of the detection of coincidences, outcomes 0 and 1 for A imply initial states $\gamma = 0, 1$ for S and occur with probability $p_\gamma = \{\delta, 1-\delta\}$.

The S photons, on the other hand, pass through an interferometer which implements an FTAD channel of the form $\Lambda[\rho_S] = \sum_{j=1}^4 E_j \rho_S E_j^\dagger$, with Kraus operators (satisfying $\sum_j E_j^\dagger E_j = \mathbb{1}$)

$$\begin{aligned} E_1 &= \sqrt{p} \begin{bmatrix} 1 & 0 \\ 0 & \sqrt{\eta} \end{bmatrix}, & E_2 &= \sqrt{p} \begin{bmatrix} 0 & \sqrt{1-\eta} \\ 0 & 0 \end{bmatrix}, \\ E_3 &= \sqrt{1-p} \begin{bmatrix} \sqrt{\eta} & 0 \\ 0 & 1 \end{bmatrix}, & E_4 &= \sqrt{1-p} \begin{bmatrix} 0 & 0 \\ \sqrt{1-\eta} & 0 \end{bmatrix}, \end{aligned} \quad (1)$$

which can be thought of as a combination of emission ($E_{1,2}$) and excitation ($E_{3,4}$) processes with coupling strength $\eta \in [0, 1]$ and probabilities p and $1-p$ [42]. The FTAD mimics a thermal bath acting on a photon, with the parameter p interpreted as the thermal occupation probability. In fact, as discussed in [12], each index $j = 1, 2, 3, 4$ can also be associated with a set composed of an initial and a final state of the reservoir.

The FTAD interferometer is implemented by entangling the photon polarization with path degrees of freedom, as sketched in Fig. 1(d). The S photons are first sent to a birefringent calcite beam displacer BD1 that transmits (deviates) the vertically (horizontally) polarized photons, creating two spatial modes (up u and down d), which we will call transversal modes (TMs). The polarization of photons in mode d is

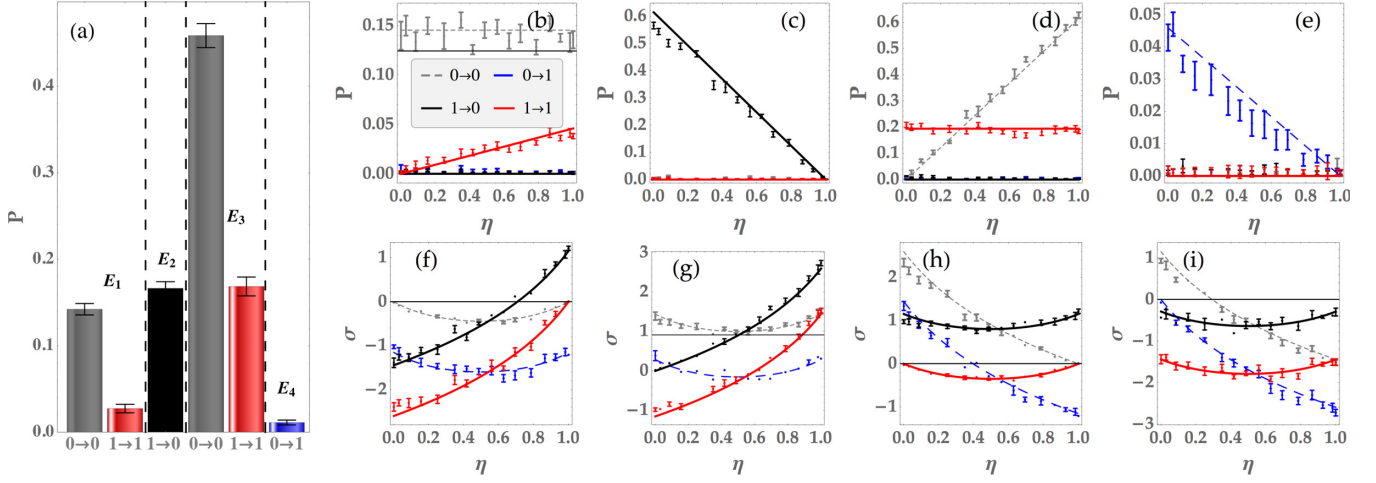


FIG. 2. Experimentally determined probabilities and entropy production for all possible stochastic trajectories. (a) Probabilities (2) for Kraus channels E_1, \dots, E_4 and the system transitions $\gamma \rightarrow \gamma'$, with $\eta = 0.7(2)$. (b)–(e) Same as in (a) but as a function of η . Each panel corresponds to a different channel E_1, \dots, E_4 and each curve to a transition $\gamma \rightarrow \gamma'$, as labeled in image (b). (f)–(i) Corresponding stochastic entropy production $\sigma[\gamma, \gamma', j]$ [Eq. (3)]. We only show curves for trajectories having $P \neq 0$ in (b)–(e). Points correspond to the experimental data, while the curves refer to the theoretical predictions. Error bars are calculated from Poissonian statistics for each outcome. In all curves $p = 0.19(1)$ and $\delta = 0.77(1)$.

rotated by a HWP at 45° and both TMs pass through a HWP, whose axis is rotated by $\phi/2$. The photons are thus reflected (transmitted) in PBS_1 with probability $p = \sin^2 \phi$ ($1 - p = \cos^2 \phi$) into the longitudinal mode (LM) long l_i (short s_i), where the set of Kraus operators $\{E_1, E_2\}$ ($\{E_3, E_4\}$) is implemented. In our setup, we tune the coupling strength of the channel with the angle $\theta/2$ of two HWPs such that $\eta = \cos^2 \theta$. Hence, both parameters of the FTAD are adjusted at will. It is worth mentioning that the interferometer in Fig. 1(d) can also implement other environments, including dephasing, bit flip, and depolarization [43,44]. Finally, the photons are sent to PBS_2 , which incoherently combines both LMs and splits the photons in the two final states of the reservoir, s_f and l_f . All HPWs in 0° serve to compensate for the path length, allowing a coherent superposition of the TMs at BD2 and BD3, necessary for the implementation E_1 and E_3 . Beam displacer BD4 plays two roles in our setup: (i) It traces out the TM and, in conjunction with the plate T, (ii) it selects photons coming from l_f or s_f , performing a projective measurement in the computational basis of the reservoir. The optical elements in the pink box are responsible for performing projective polarization measurements, yielding final outcomes $\gamma' = 0, 1$. The joint distribution $P(\gamma, \gamma')$ is then obtained by registering coincidence counts between Det1 and Det2.

As discussed above and formally demonstrated in the Supplemental Material [12], each Kraus operator E_j is associated with a specific optical path. Crucially, by blocking three out of the four paths, we can thus also determine $P(\gamma, \gamma', j)$, which represents the joint probability that the system undergoes a transition from $\gamma \rightarrow \gamma'$ in path $j = 1, 2, 3, 4$, which is given by

$$P(\gamma, \gamma', j) = p_\gamma |\langle \gamma' | E_j | \gamma \rangle|^2. \quad (2)$$

Thermodynamically, this would be tantamount to the joint TPM distribution of both the system and bath, where the index j collectively describes the initial and final states of the

bath. In our case, this bath is represented instead by the path degrees of freedom of the interferometer.

The experimentally obtained probabilities are shown in Fig. 2 for fixed $p = 0.19(1)$ and $\delta = 0.77(1)$. The image in Fig. 2(a) summarizes all probabilities which are nonzero, with fixed $\eta = 0.7(2)$. In fact, out of the possible 16 outcomes (γ, γ', j) , only six are not zero. This is because E_1 and E_3 do not generate jumps and hence allow only for the transitions $0 \rightarrow 0$ and $1 \rightarrow 1$ in the system. Conversely, E_2 and E_4 necessarily cause the system to jump, from 1 to 0 and from 0 to 1, respectively. This is a manifestation of the preservation of the total number of excitations in the system and bath. Figures 2(b)–2(e) depict the probabilities as a function of η , each plot corresponding to a different Kraus channel E_j . For comparison, the theoretical predictions from Eq. (2) are also shown. In all cases, the fidelity (Bhattacharyya distance) between theory and experiment is above 0.98, therefore confirming that the TPM protocol was successfully implemented.

III. STOCHASTIC ENTROPY PRODUCTION

The stochastic entropy production along a trajectory (γ, γ', j) reads [37,45,46]

$$\sigma(\gamma, \gamma', j) = \ln(p_\gamma / \tilde{p}_{\gamma'}) + \Phi_j, \quad (3)$$

where $\tilde{p}_{\gamma'} = \sum_{\gamma, j} P(\gamma, \gamma', j)$ is the probability associated with the final state of S . The first term in (3) represents the stochastic variation in the system's entropy. Indeed, averaging over Eq. (2) leads to $\langle \ln p_\gamma / \tilde{p}_{\gamma'} \rangle = S(\Lambda[\rho_S]) - S(\rho_S)$, where $S(\rho) = -\text{tr}(\rho \ln \rho)$ is the von Neumann entropy. The second term in Eq. (3) is the entropy flux Φ_j to the reservoir. It therefore depends only on the path j the photon undergoes (and not on γ and γ'). These fluxes are associated with quantum jumps in the system [45]. Since E_1 and E_3 involve no jumps, we have $\Phi_1 = \Phi_3 = 0$. Conversely, paths 2 and 4 must be accompanied by finite fluxes Φ_2 and Φ_4 , since they involve jumps from 1 to 0 and from 0 to 1, respectively. To determine Φ_2 and

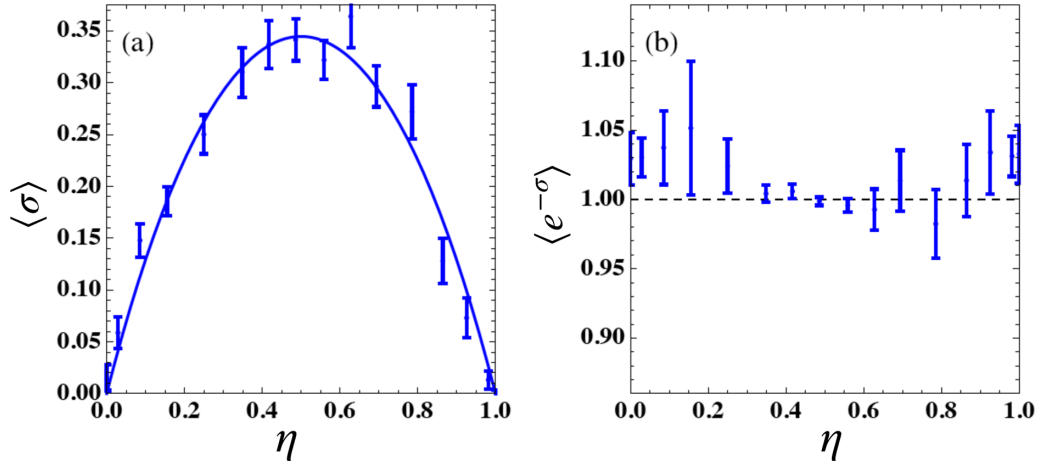


FIG. 3. (a) Average entropy production $\langle \sigma \rangle$ and (b) fluctuation theorem $\langle e^{-\sigma} \rangle$ as a function of η for $p = 0.19(1)$.

Φ_4 we use the fact that the time-reversed Kraus operators \tilde{E}_j should be related to the forward Kraus operators according to $\tilde{E}_j = e^{-\Phi_j/2} E_j^\dagger$ [37,47]. For the FTAD this yields the unique solution $\Phi_2 = -\Phi_4 = \ln p/(1-p)$. With these expressions for Φ_j , it then follows from Eq. (3) that σ satisfies the integral fluctuation theorem

$$\langle e^{-\sigma} \rangle = 1. \quad (4)$$

The experimentally determined values of the stochastic entropy production (3) are shown in Figs. 2(f)–2(i) as a function of η for fixed $p = 0.19(1)$ and $\delta = 0.77(1)$. Each plot corresponds to a different channel j of the FTAD. For some trajectories the corresponding probabilities [Figs. 2(b)–2(e)] are identically zero, so these values will not contribute to any averages. For instance, because of Fig. 2(b), in Fig. 2(f) the only values of σ which will actually play a nontrivial role are those corresponding to the trajectories $0 \rightarrow 0$ and $1 \rightarrow 1$ (gray and red curves).

As can be seen in Figs. 2(f)–2(i), at the stochastic level some of the entropy productions can be negative. This does not contradict the second law, which holds only at the level of averages. Indeed, from Eq. (4) and Jensen's inequality, it follows that $\langle \sigma \rangle \geq 0$. This means that negative values are less likely, which can be observed by comparing the probabilities in Figs. 2(b)–2(e). The average entropy production $\langle \sigma \rangle = \sum_{\gamma, \gamma', j} \sigma(\gamma, \gamma', j) P(\gamma, \gamma', j)$ is shown in Fig. 3(a), together with the fluctuation theorem (4) in Fig. 3(b). In both cases, the experiment confirms the experimental predictions: $\langle \sigma \rangle \geq 0$ and $\langle e^{-\sigma} \rangle = 1$.

IV. CONCLUSION

Thermodynamic quantities, such as heat, work, or entropy production, characterize transformations (i.e., processes) that the system undergoes. However, directly assessing processes in quantum systems is notoriously difficult. We have demonstrated a platform that overcomes this by implementing a photonics simulation of a two-level system interacting with a thermal reservoir. The key feature of our setup is the ability to obtain the full TPM statistics of both the system and bath, directly from the clicks of an experiment. This was

accomplished by combining two features. First, the configurations of the reservoir are characterized by a set of Kraus operators, each corresponding to a specific optical path of the interferometer. Hence, by blocking three out of the four paths, we could directly study the statistics conditioned on each bath configuration. Second, we used entangled photon pairs to nondestructively measure the initial system configuration. Combined with the final measurement, associated with the photon that went through the interferometer, this yields the full TPM statistics of both the system and bath.

As a proof of principle, we have focused on the entropy production in a heat exchange process. This is convenient since entropy production is a fully information-theoretic quantity and hence avoids entering issues about the energetics of photon processes. However, our approach is highly flexible and can be extended to various other thermodynamic protocols, including systems with initial coherences. The latter in particular would be an interesting direction for future research, since the TPM becomes invasive in the presence of energetic coherences [14,16–21]. Our framework can be readily extended to include initial coherences in the system, for example, by rotating the initial states of the entangled pair. These could be used to compare the TPM with other alternatives that have recently been proposed to overcome this invasiveness, such as Bayesian networks [19] and quasiprobabilities [17,48].

ACKNOWLEDGMENTS

We thank S. Walborn for valuable discussions. The authors acknowledge financial support from the Brazilian agencies CNPq (PQ Grants No. 305740/2016-4, No. 307058/2017-4, No. 309020/2020-4, and No. INCT-IQ 246569/2014-0). G.T.L. acknowledge financial support from the São Paulo Funding Agency FAPESP (Grants No. 2017/50304-7, No. 2017/07973-5, and No. 2018/12813-0). G.H.A. acknowledges FAPERJ (Grant No. JCNE E-26/201.355/2021) and FAPESP (Grant No. 2021/96774-4). T.L.S. would like to thank Serrapilheira Institute (Grant No. Serra-1709-17173). This work was realized as part of the CAPES/PROCAD program.

G.H.A. and T.L.S. contributed equally to this work.

- [1] G. Gallavotti and E. G. D. Cohen, *J. Stat. Phys.* **80**, 931 (1995).
- [2] D. J. Evans, E. G. D. Cohen, and G. P. Morriss, *Phys. Rev. Lett.* **71**, 2401 (1993).
- [3] G. E. Crooks, *J. Stat. Phys.* **90**, 1481 (1998).
- [4] C. Jarzynski, *J. Stat. Phys.* **96**, 415 (1999).
- [5] J. Lebowitz and H. Spohn, *J. Stat. Phys.* **95**, 333 (1999).
- [6] J. Liphardt, S. Dumont, S. B. Smith, I. Tinoco, and C. Bustamante, *Science* **296**, 1832 (2002).
- [7] D. Collin, F. Ritort, C. Jarzynski, S. B. Smith, I. Tinoco, and C. Bustamante, *Nature (London)* **437**, 231 (2005).
- [8] J. R. Gomez-Solano, A. Petrosyan, and S. Ciliberto, *Phys. Rev. Lett.* **106**, 200602 (2011).
- [9] P. Talkner, E. Lutz, and P. Hänggi, *Phys. Rev. E* **75**, 050102(R) (2007).
- [10] M. Esposito, U. Harbola, and S. Mukamel, *Rev. Mod. Phys.* **81**, 1665 (2009).
- [11] M. Campisi, P. Hänggi, and P. Talkner, *Rev. Mod. Phys.* **83**, 771 (2011).
- [12] See Supplemental Material at <http://link.aps.org/supplemental/10.1103/PhysRevA.106.L020201> for details.
- [13] A. E. Allahverdyan, *Phys. Rev. E* **90**, 032137 (2014).
- [14] J. Åberg, *Phys. Rev. X* **8**, 011019 (2018).
- [15] P. Solinas and S. Gasparinetti, *Phys. Rev. E* **92**, 042150 (2015).
- [16] M. Perarnau-Llobet, E. Bäumer, K. V. Hovhannisyan, M. Huber, and A. Acin, *Phys. Rev. Lett.* **118**, 070601 (2017).
- [17] A. Levy and M. Lostaglio, *PRX Quantum* **1**, 010309 (2020).
- [18] S. Gherardini, A. Belenchia, M. Paternostro, and A. Trombettoni, *Phys. Rev. A* **104**, L050203 (2021).
- [19] K. Micadei, G. T. Landi, and E. Lutz, *Phys. Rev. Lett.* **124**, 090602 (2020).
- [20] S. Deffner, J. P. Paz, and W. H. Zurek, *Phys. Rev. E* **94**, 010103(R) (2016).
- [21] A. Sone, Y.-x. Liu, and P. Cappellaro, *Phys. Rev. Lett.* **125**, 060602 (2020).
- [22] S. An, J.-N. Zhang, M. Um, D. Lv, Y. Lu, J. Zhang, Z.-Q. Yin, H. T. Quan, and K. Kim, *Nat. Phys.* **11**, 193 (2015).
- [23] S. Hernández-Gómez, S. Gherardini, F. Poggiali, F. S. Cataliotti, A. Trombettoni, P. Cappellaro, and N. Fabri, *Phys. Rev. Research* **2**, 023327 (2020).
- [24] R. M. de Araújo, T. Häffner, R. Bernardi, D. S. Tasca, M. P. J. Lavery, M. J. Padgett, A. Kanaan, L. C. Céleri, and P. H. S. Ribeiro, *J. Phys. Commun.* **2**, 035012 (2018).
- [25] M. A. A. Talarico, P. B. Monteiro, E. C. Mattei, E. I. Duzzioni, P. H. Souto Ribeiro, and L. C. Céleri, *Phys. Rev. A* **94**, 042305 (2016).
- [26] T. B. Batalhão, A. M. Souza, L. Mazzola, R. Aucaise, R. S. Sarthour, I. S. Oliveira, J. Goold, G. De Chiara, M. Paternostro, and R. M. Serra, *Phys. Rev. Lett.* **113**, 140601 (2014); T. B. Batalhão, A. M. Souza, R. S. Sarthour, I. S. Oliveira, M. Paternostro, E. Lutz, and R. M. Serra, *ibid.* **115**, 190601 (2015).
- [27] P. A. Camati, J. P. S. Peterson, T. B. Batalhão, K. Micadei, A. M. Souza, R. S. Sarthour, I. S. Oliveira, and R. M. Serra, *Phys. Rev. Lett.* **117**, 240502 (2016).
- [28] L. Mazzola, G. De Chiara, and M. Paternostro, *Phys. Rev. Lett.* **110**, 230602 (2013).
- [29] R. Dörner, S. R. Clark, L. Heaney, R. Fazio, J. Goold, and V. Vedral, *Phys. Rev. Lett.* **110**, 230601 (2013).
- [30] A. J. Roncaglia, F. Cerisola, and J. P. Paz, *Phys. Rev. Lett.* **113**, 250601 (2014).
- [31] F. Cerisola, Y. Margalit, S. MacHluf, A. J. Roncaglia, J. P. Paz, and R. Folman, *Nat. Commun.* **8**, 1241 (2017).
- [32] M. Naghiloo, D. Tan, P. M. Harrington, J. J. Alonso, E. Lutz, A. Romito, and K. W. Murch, *Phys. Rev. Lett.* **124**, 110604 (2020); M. Naghiloo, J. J. Alonso, A. Romito, E. Lutz, and K. W. Murch, *ibid.* **121**, 030604 (2018).
- [33] Y. Masuyama, K. Funo, Y. Murashita, A. Noguchi, S. Kono, Y. Tabuchi, R. Yamazaki, M. Ueda, and Y. Nakamura, *Nat. Commun.* **9**, 1291 (2018).
- [34] S. Pal, T. S. Mahesh, and B. K. Agarwalla, *Phys. Rev. A* **100**, 042119 (2019).
- [35] C. Jarzynski and D. K. Wójcik, *Phys. Rev. Lett.* **92**, 230602 (2004).
- [36] S. Jevtic, T. Rudolph, D. Jennings, Y. Hirono, S. Nakayama, and M. Murao, *Phys. Rev. E* **92**, 042113 (2015).
- [37] G. Manzano, J. M. Horowitz, and J. M. R. Parrondo, *Phys. Rev. X* **8**, 031037 (2018).
- [38] J. P. Santos, L. C. Céleri, G. T. Landi, and M. Paternostro, *npj Quantum Inf.* **5**, 23 (2019).
- [39] A. Solfanelli, A. Santini, and M. Campisi, *PRX Quantum* **2**, 030353 (2021).
- [40] P. H. Souto Ribeiro, T. Häffner, G. L. Zanin, N. Rubiano da Silva, R. Medeiros de Araújo, W. C. Soares, R. J. de Assis, L. C. Céleri and A. Forbes, *Phys. Rev. A* **101**, 052113 (2020).
- [41] P. G. Kwiat, E. Waks, A. G. White, I. Appelbaum, and P. H. Eberhard, *Phys. Rev. A* **60**, R773(R) (1999).
- [42] M. Nielsen and I. Chuang, *Quantum Computation and Quantum Information* (Cambridge University Press, Cambridge, 2000).
- [43] G. H. Aguilar, A. Valdés-Hernández, L. Davidovich, S. P. Walborn, and P. H. Souto Ribeiro, *Phys. Rev. Lett.* **113**, 240501 (2014).
- [44] G. H. Aguilar, O. J. Farías, A. Valdés-Hernández, P. H. Souto Ribeiro, L. Davidovich, and S. P. Walborn, *Phys. Rev. A* **89**, 022339 (2014).
- [45] H. P. Breuer, *Phys. Rev. A* **68**, 032105 (2003).
- [46] G. T. Landi and M. Paternostro, *Rev. Mod. Phys.* **93**, 035008 (2021).
- [47] G. E. Crooks, *Phys. Rev. A* **77**, 034101 (2008).
- [48] N. Yunger Halpern, B. Swingle, and J. Dressel, *Phys. Rev. A* **97**, 042105 (2018).